

Prospects for the measurement of B_s^0 oscillations with the ATLAS detector at LHC

B. Epp, V.M. Ghete, A. Nairz

Institute for Experimental Physics, University of Innsbruck, Austria

January 31, 2002

Abstract. The capabilities of the ATLAS detector to measure the B_s^0 oscillations in proton-proton interactions at the Large Hadron Collider were evaluated. B_s^0 candidates in the $D_s^- \pi^+$ and $D_s^- a_1^+$ decay modes from semileptonic exclusive events were fully simulated and reconstructed, using a detailed detector description. The sensitivity and the expected accuracy for the measurement of the oscillation frequency were derived from unbinned maximum likelihood amplitude fits as functions of the integrated luminosity. A detailed treatment of the systematic uncertainties was performed. The dependence of the measurement sensitivity on various parameters was also evaluated.

1 Introduction

The observed B_s^0 and \bar{B}_s^0 states are linear combinations of two mass eigenstates, denoted here as H and L . Due to the non-conservation of flavour in charged weak-current interactions, transitions between B_s^0 and \bar{B}_s^0 states occur with a frequency proportional to $\Delta m_s = m_H - m_L$.

Experimentally, these $B_s^0 - \bar{B}_s^0$ oscillations have not yet been observed directly. In the Standard Model, their frequency is predicted in Ref. [1] to be between 12.0 ps^{-1} and 17.6 ps^{-1} with 68% CL, and lower than 20 ps^{-1} at 95% CL, significantly larger than the corresponding value Δm_d in the $B_d^0 - \bar{B}_d^0$ system. From measurements done by the ALEPH, DELPHI and OPAL experiments at LEP, by SLD at SLC, and by CDF at the Tevatron, a combined lower bound of $\Delta m_s > 18.0 \text{ ps}^{-1}$ has been established at 95% CL [2]. In the $B_d^0 - \bar{B}_d^0$ system, the oscillations have been directly observed and a rather precise value of $\Delta m_d = 0.472 \pm 0.017 \text{ ps}^{-1}$ [3] has been measured.

The values for Δm_d and Δm_s predicted in the Standard Model by computing the corresponding box diagrams, with the top-quark contribution assumed to be dominant, are proportional to $|V_{td}|^2$ and $|V_{ts}|^2$ respectively. The direct determination of V_{td} and V_{ts} from Δm_d and Δm_s is, however, hampered by hadronic uncertainties. These uncertainties partially cancel in the ratio:

$$\frac{\Delta m_s}{\Delta m_d} = \frac{M_{B_s^0}}{M_{B_d^0}} \frac{\hat{B}_{B_s^0} f_{B_s^0}^2}{\hat{B}_{B_d^0} f_{B_d^0}^2} \left| \frac{V_{ts}}{V_{td}} \right|^2,$$

where M_B are the B -meson masses, \hat{B}_B are the bag parameters, and f_B are the B -meson form factors. Using the experimentally-measured masses and a value for the ratio $\xi = \sqrt{\hat{B}_{B_s^0} f_{B_s^0}} / \sqrt{\hat{B}_{B_d^0} f_{B_d^0}}$ which can be computed in lattice QCD, a better constraint for V_{ts}/V_{td} can be obtained,

which can then be converted into a constraint of $|V_{td}|$, the worst-measured side of the unitarity triangle.

In this note, an evaluation of the capability of the ATLAS detector to measure the B_s^0 oscillations in proton-proton interactions at the Large Hadron Collider (LHC) is presented. Some quantities involved in the measurement are still uncertain (cross sections, shape of the background, the final characteristics of the detector), therefore the dependence of the measurement sensitivity and of the expected accuracy on these parameters is also evaluated.

2 Event selection

The signal channels considered in this analysis for the measurement of $B_s^0 - \bar{B}_s^0$ oscillations are $B_s^0 \rightarrow D_s \pi$ and $B_s^0 \rightarrow D_s a_1$, with $D_s \rightarrow \phi \pi$ followed by $\phi \rightarrow K^+ K^-$.

The event samples were generated using PYTHIA 5.7 [4], passed then through the ATLAS full GEANT-based simulation program DICE (Inner Detector (ID) only) and reconstructed using an algorithm based on the Kalman filter implemented in the xKalman package from the ATLAS reconstruction program ATRECON. The physics model used for simulation, the description of the detector and of the reconstruction program are presented in detail in Ref. [5].

In the simulation, b -quark pairs were produced in pp -collisions at $\sqrt{s} = 14 \text{ TeV}$ by including direct production, gluon splitting and flavour excitation processes for $b\bar{b}$ production. The b -quark was forced to decay semileptonically giving a muon with transverse momentum¹ $p_T > 6 \text{ GeV}$

¹ The coordinate system has the z direction along the beam axis, with x -axis pointing to the centre of the accelerator ring and y -axis pointing upwards. The transverse momenta are computed with respect to the z axis.

and pseudo-rapidity $|\eta| < 2.4$ which is used by the level-1 trigger to select the B hadronic channels in ATLAS. The associated \bar{b} was forced to produce the required B -decay channels. All the charged final-state particles from the B decay were required to have $p_T > 0.5$ GeV and $|\eta| < 2.5$.

The reconstruction of the B_s^0 vertex proceeded via the following steps (charge-conjugate states are implicitly included). The ϕ decay vertex was first reconstructed by considering all combinations of pairs of oppositely-charged tracks with $p_T > 1.5$ GeV for both tracks. Kinematic cuts on the angles between the two tracks $\Delta\varphi_{KK} < 10^\circ$ and $\Delta\theta_{KK} < 10^\circ$ were also imposed. Here φ denotes the azimuthal angle and θ the polar angle in the coordinate system defined previously. The two-track vertex was then fitted assigning the kaon mass to both tracks. Combinations passing a fit-probability [6] cut of 1% with the invariant mass within $3\sigma_\phi$ of the nominal ϕ mass were selected as ϕ candidates. To all accepted ϕ candidates, a third negative track with $p_T > 1.5$ GeV from the remaining ones was added. The pion mass was assigned to the third track and a three-track vertex was refitted. Combinations of three tracks which had a fit probability greater than 1% and an invariant mass within $3\sigma_{D_s^-}$ of the nominal D_s^- mass were selected as D_s^- candidates.

For each reconstructed D_s^- meson, a search was made for a_1^+ candidates in three-particle combinations of the remaining charged tracks. In a first step, ρ^0 mesons were reconstructed from all combinations of two tracks with opposite charges and with $p_T > 0.5$ GeV for both tracks, each particle in the combination being assumed to be a pion. Kinematic cuts $\Delta\theta_{\pi\pi} < 15^\circ$ and $\Delta\varphi_{\pi\pi} < 35^\circ$ were used to reduce the combinatorial background. The two selected tracks were then fitted as originating from the same vertex; from the combinations passing a fit probability cut of 1%, those with an invariant mass within $1.5 \Gamma_{BW}$ of the nominal ρ^0 mass were selected as ρ^0 candidates. Next, a positive track with $p_T > 0.5$ GeV from the remaining charged tracks was added to the ρ^0 candidate, assuming the pion hypothesis for the extra track. The three tracks were then fitted as originating from a common vertex, without any mass constraints. Combinations with a fit probability greater than 1% and with an invariant mass within 300 MeV of the nominal a_1 mass were selected as a_1^+ candidates.

For the $B_s^0 \rightarrow D_s^- \pi^+$ channel, the B_s^0 decay vertex was reconstructed by considering all D_s^- candidates and adding a fourth track from the remaining tracks in the event. This track was required to have opposite charge with respect to the pion track from the D_s^- and $p_T > 1$ GeV. The four-track decay vertex was refitted including ϕ and D_s^- mass constraints, and requiring that the total momentum of the B_s^0 vertex pointed to the primary vertex (within the primary vertex spatial resolutions of $\sigma_x = \sigma_y = 28 \mu\text{m}$ and $\sigma_z = 46 \mu\text{m}$) and the momentum of D_s^- vertex pointed to the B_s^0 vertex.

For the $B_s^0 \rightarrow D_s^- a_1^+$ channel, the B_s^0 candidates were reconstructed combining the D_s^- candidates with the a_1^+ candidates. A six-track vertex fit was then performed with mass constraints for the tracks from ϕ and D_s^- ; due to the

large a_1 natural width, the three tracks from the a_1^+ were not constrained to a_1 mass. As in the $B_s^0 \rightarrow D_s^- \pi^+$ channel, the total momentum of the B_s^0 vertex was required to point to the primary vertex and the momentum of D_s^- vertex was required to point to the B_s^0 vertex.

In order to be selected as B_s^0 candidates, the four-track and six-track combinations were required to give a probability greater than 1% for the vertex fit. The signed separation between the reconstructed B_s^0 vertex and the primary vertex, and between the D_s^- and B_s^0 vertex were required to be positive (the momentum should not point backward to the parent vertex). To improve the purity of the sample, further cuts were imposed: the accepted B_s^0 candidates were required to have a proper decay time greater than 0.4 ps, an impact parameter smaller than $55 \mu\text{m}$ and $p_T > 10$ GeV.

Background to the channels being considered for the measurement of Δm_s can come from two sources: from other four- or six-body B -hadron decay channels, and from combinatorial background (random combinations with some or all particles not originating from a B decay). For $B_s^0 \rightarrow D_s^- \pi^+$, the following four-body decay channels were considered as potential sources of background: $\bar{B}_d^0 \rightarrow D_s^- \pi^+$, $B_d^0 \rightarrow D^- \pi^+$ (with D^- , $D_s^- \rightarrow \phi \pi^-$ and $\phi \rightarrow K^+ K^-$) and $\Lambda_b^0 \rightarrow \Lambda_c^+ \pi^-$ followed by $\Lambda_c^+ \rightarrow p K^- \pi^+$. The similar six-body decay channels considered as potential sources of background for $B_s^0 \rightarrow D_s^- a_1^+$ were: $\bar{B}_d^0 \rightarrow D_s^- a_1^+$, $B_d^0 \rightarrow D^- a_1^+$ (with D^- , $D_s^- \rightarrow \phi \pi^-$ and $\phi \rightarrow K^+ K^-$) and $\Lambda_b^0 \rightarrow \Lambda_c^+ \pi^-$ followed by $\Lambda_c^+ \rightarrow p K^- \pi^+ \pi^+ \pi^-$. The simulated four- and six-body background events were passed through the detailed detector-simulation program, reconstructed and analysed using the same programs, the same conditions and the same cuts as the signal events.

In order to study the combinatorial background, a very large sample of simulated inclusive-muon events is needed. The results presented here are based on a sample of 1.1 million $b\bar{b} \rightarrow \mu X$ events, with $p_T > 6$ GeV and $|\eta| < 2.4$ for the muon corresponding to the trigger conditions.

The $b\bar{b} \rightarrow \mu X$ sample was analysed in the framework of a fast-simulation program ATLFast++ [5], applying the same algorithms and the same cuts that were used for the fully-simulated samples. A careful check was made of the performance of the fast-simulation program by running it on signal and background samples, and comparing the results with those from the detailed simulation. Reasonable agreement was obtained for the number of reconstructed events and the widths of the mass peaks for the reconstructed particles.

A multi-level trigger is used to select the events for this analysis. The level-1 trigger is the inclusive muon trigger mentioned before. The level-2 trigger [7] reconfirms the muon from level-1 trigger, then in an un-guided search for tracks in the Inner Detector reconstructs a ϕ meson and, adding a new track, a D_s meson. The level-2 trigger uses dedicated online software. 63% of the signal events selected offline pass the level-2 trigger cuts; from the $b\bar{b} \rightarrow \mu X$ sample, $(3.4 \pm 0.2)\%$ of the events are selected. The level-3 trigger (the event filter) uses a set of loose offline

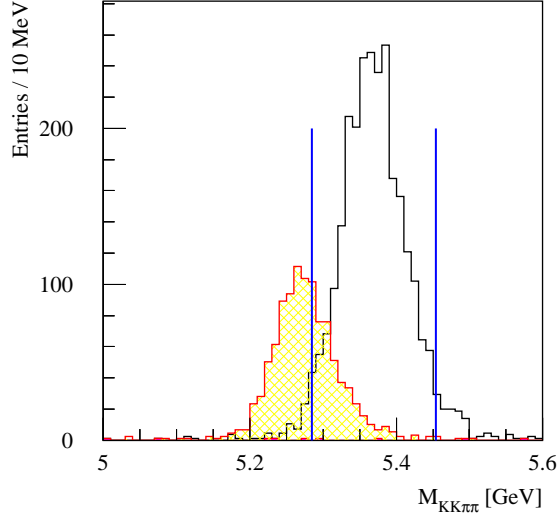


Fig. 1. Reconstructed B_s^0 invariant-mass distribution for $B_s^0 \rightarrow D_s^- \pi^+$ decays. The open histogram shows the signal, the hatched histogram the background from $\bar{B}_d^0 \rightarrow D_s^- \pi^+$ decays, and the dark histogram the fake reconstructed decays from the signal sample. The combinatorial background is not shown here.

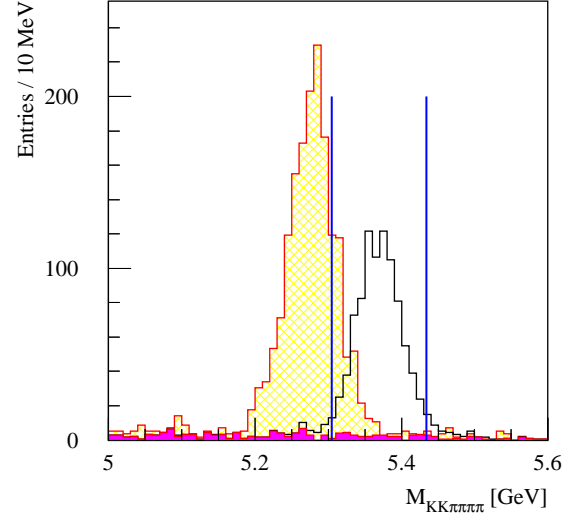


Fig. 2. Reconstructed B_s^0 invariant-mass distribution for $B_s^0 \rightarrow D_s^- a_1^+$ decays. The open histogram shows the signal, the hatched histogram the background from $\bar{B}_d^0 \rightarrow D_s^- a_1^+$ decays, and the dark histogram the fake reconstructed decays from the signal sample. The combinatorial background is not shown here.

Process	Cross-section (pb)	Effective cross-section (pb)	Simulated events	Rec. events	Rec. events for 10 fb ⁻¹
$B_s^0 \rightarrow D_s^- \pi^+$	12.81	5.24	23893	2088	2370
$\bar{B}_d^0 \rightarrow D_s^- \pi^+$	4.52	2.08	9989	369	400
$B_d^0 \rightarrow D^- \pi^+$	8.21	3.74	9989	2	3
$\Lambda_b^0 \rightarrow \Lambda_c^+ (p K^- \pi^+) \pi^-$	89.44	2.27	9989	1	2
$B_s^0 \rightarrow D_s^- a_1^+$	12.81	2.08	18784	1512	870
$\bar{B}_d^0 \rightarrow D_s^- a_1^+$	20.98	3.35	9699	190	340
$B_d^0 \rightarrow D^- a_1^+$	8.20	1.40	9949	1	1
$\Lambda_b^0 \rightarrow \Lambda_c^+ (p K^- \pi^+ \pi^+ \pi^-) \pi^-$	1.97	0.20	10994	0	0
Comb. background sum			1.1×10^6	see text	3750

Table 1. Signal and background samples analysed for the study of B_s^0 - \bar{B}_s^0 oscillations. The combinatorial background is the sum for both $B_s^0 \rightarrow D_s^- \pi^+$ and $B_s^0 \rightarrow D_s^- a_1^+$ analysis channels.

cuts, reducing the rate to $(0.26 \div 0.41)\%$ of the μX rate, depending on the actual values which are set for the cuts.

The reconstructed B_s^0 invariant-mass distributions in the decay channels $B_s^0 \rightarrow D_s^- \pi^+$ and $B_s^0 \rightarrow D_s^- a_1^+$ are shown in Figure 1 and Figure 2, respectively, for an integrated luminosity of 10 fb⁻¹.

The numbers of events expected for the various signal and background channels that have been analysed are given in Table 1 for an integrated luminosity of 10 fb⁻¹. The first cross-section column in Table 1 gives the channel cross-section, without any cuts on final-state particles, assuming a cross-section of 2.3 μb for the process $b\bar{b} \rightarrow \mu(p_T > 6 \text{ GeV}, |\eta| < 2.4)X$. The effective cross-section is the cross-section after the cuts on charged final-state particles were applied during simulation.

The events reconstructed from the samples for the exclusive decay modes were counted in a $\pm 2\sigma$ window

around the nominal B_s^0 mass. Using the fraction of events reconstructed in the simulated sample and the number of events expected for an integrated luminosity of 10 fb⁻¹, the expected number of reconstructed events was estimated. Corrections for muon efficiency (on average 0.82) and for level-2 trigger efficiency (0.63) were also applied.

A total of 3240 reconstructed events is expected for the $B_s^0 \rightarrow D_s \pi$ and $B_s^0 \rightarrow D_s a_1$ decay channels for an integrated luminosity of 10 fb⁻¹.

The only significant background comes from the $\bar{B}_d^0 \rightarrow D_s^- \pi^+$ and $\bar{B}_d^0 \rightarrow D_s^- a_1^+$ channels, and from the combinatorial background. Note that the number of reconstructed events from the two decay channels is conservative since the branching-ratio values used are upper limits. As expected, due to the combination of the D^- mass shift ($M_{D^-} - M_{D_s^-} = 90 \text{ MeV}$) and B_d^0 mass shift ($M_{B_s^0} - M_{B_d^0} \approx 100 \text{ MeV}$), very few $B_d^0 \rightarrow D^- a_1^+$, $D^- \pi^+$

events are reconstructed in a $\pm 2\sigma$ window around B_s^0 nominal mass. Due to the different decay topology, the $A_b^0 \rightarrow A_c^+ \pi^-$ channel does not give any contribution to the background.

The statistics available for estimating the combinatorial background are very limited, despite the large size (1.1 million events) of the μX sample. Each simulated event was therefore passed 50 times through the fast-simulation program, different random smearing of the track parameters being applied each time. The number of background events was counted in a 2σ mass window around the B_s^0 nominal mass. On average, 0.12 events per pass were reconstructed in the mass window, summing the $B_s^0 \rightarrow D_s^- \pi^+$ and $B_s^0 \rightarrow D_s^- a_1^+$ channels. Normalising to the number of μX events expected for an integrated luminosity of 10 fb^{-1} , applying correction factors for the reconstruction and trigger efficiencies, the combinatorial background was estimated to be 3752 events, and the range of variation was estimated to be between 2079 and 5425 events at 90% CL. Correlations between the results from the 50 passes were taken into account.

3 Proper-time reconstruction and resolution

The proper time of the reconstructed B_s^0 candidates was computed from the reconstructed transverse decay length, d_{xy} , and from the B_s^0 transverse momentum, p_T :

$$t = \frac{d_{xy} M_{B_s^0}}{c p_T} \equiv d_{xy} g$$

where $g = M_{B_s^0}/(c p_T)$.

The transverse decay length is the distance between the interaction point and the b -hadron decay vertex, projected onto the transverse plane. Figure 3 shows, for the example of the $B_s^0 \rightarrow D_s^- (\phi \pi^-) \pi^+$ decay mode, the difference $d_{xy} - d_{xy}^0$ fitted with two Gaussian functions, where d_{xy}^0 is the true transverse decay length. For each event, the decay-length uncertainty, $\sigma_{d_{xy}}$, was estimated from the covariance matrices of the tracks associated with the vertices. The pull of the transverse decay length, $(d_{xy} - d_{xy}^0)/\sigma_{d_{xy}}$, was found to have a Gaussian shape with a width of $S_{d_{xy}} = 0.959 \pm 0.017$ for the $B_s^0 \rightarrow D_s^- \pi^+$ channel and $S_{d_{xy}} = 0.954 \pm 0.020$ for the $B_s^0 \rightarrow D_s^- a_1^+$ channel.

The distributions for $(g - g_0)/g_0$ also have a Gaussian shape for both B_s^0 decay channels, with a width of $S_g = (0.715 \pm 0.014)\%$ for the $B_s^0 \rightarrow D_s^- \pi^+$ channel and $S_g = (0.636 \pm 0.013)\%$ for the $B_s^0 \rightarrow D_s^- a_1^+$ channel. Here $g_0 = t_0/d_{xy}^0$, with t_0 being the true proper time. The $(g - g_0)/g_0$ distribution for the $B_s^0 \rightarrow D_s^- (\phi \pi^-) \pi^+$ decay mode is shown in Figure 4.

The proper-time resolution function $\text{Res}(t | t_0)$ was parametrised with the sum of two Gaussian functions, with parameters given in Table 2:

$$\text{Res}(t | t_0) = f_1 \frac{1}{\sigma_1 \sqrt{2\pi}} \exp\left(-\frac{(t - t_0)^2}{2\sigma_1^2}\right) + f_2 \frac{1}{\sigma_2 \sqrt{2\pi}} \exp\left(-\frac{(t - t_0)^2}{2\sigma_2^2}\right)$$

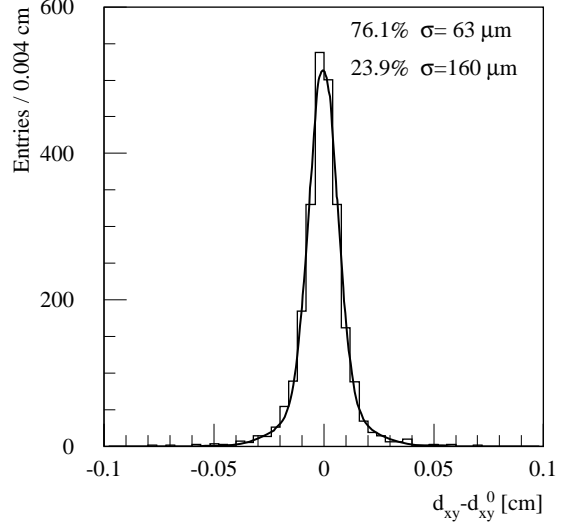


Fig. 3. Decay-radius resolution for the decay channel $B_s^0 \rightarrow D_s^- (\phi \pi^-) \pi^+$.

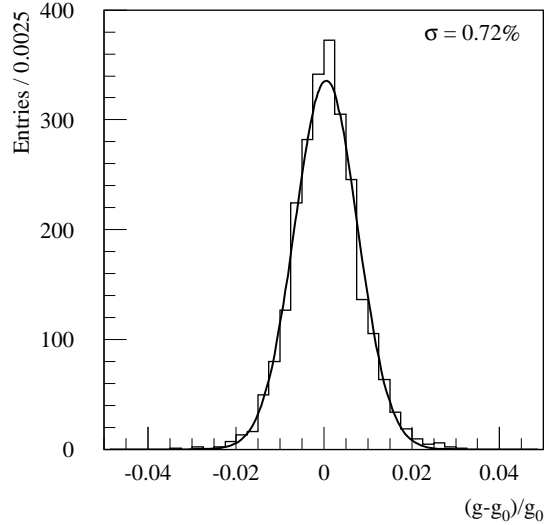


Fig. 4. Fractional resolution on g -factor for the decay channel $B_s^0 \rightarrow D_s^- (\phi \pi^-) \pi^+$.

Figures 5 and 6 show, for the decay channels $B_s^0 \rightarrow D_s^- \pi^+$ and $B_s^0 \rightarrow D_s^- a_1^+$, the proper-time resolution together with the parametrization obtained from the function given above. The distributions show deviations from the Gaussian shape, illustrated by the significant fraction of the second, broader Gaussian function in the parametrization function. For B_d^0 mesons, the ratio of the two Gaussian functions was fixed to the ratio from B_s^0 parametrization.

The parametrization chosen above reproduces well the tails seen in the distribution for reconstructed events. It has the advantage that the integrals in the log-likelihood function given in Eq. (3) can be computed analytically, much faster than the numerical computation. The depen-

α	$B_s^0 \rightarrow D_s^- \pi^+$		$B_s^0 \rightarrow D_s^- a_1^+$	
	Fraction f_α (%)	Width σ_α (fs)	Fraction f_α (%)	Width σ_α (fs)
1	59.6 ± 6.6	51.5 ± 4.0	62.5 ± 14.1	51.6 ± 6.4
2	40.4 ± 6.6	107.3 ± 8.5	37.5 ± 14.1	92.8 ± 12.7
	$B_d^0 \rightarrow D_s^- \pi^+$		$B_d^0 \rightarrow D_s^- a_1^+$	
	Fraction f_α (%)	Width σ_α (fs)	Fraction f_α (%)	Width σ_α (fs)
1	59.6 ± 1.8	56.9 ± 5.5	62.5 ± 2.6	60.3 ± 7.2
2	40.4 ± 1.8	102.9 ± 9.6	37.5 ± 2.6	100.1 ± 31.6

Table 2. Proper-time resolution function $\text{Res}(t|t_0)$ parametrization with the sum of two Gaussian functions.

dence of the proper-time resolution on the proper time $\sigma(t_0) = \sqrt{(gS_{d_{xy}}\sigma_{d_{xy}})^2 + (t_0 S_g)^2}$ can be neglected in the first approximation, as the factor S_g is very small.

4 Likelihood function

The probability density to observe an initial B_j^0 meson ($j = d, s$) decaying at time t_0 after its creation as a \bar{B}_j^0 meson is given by:

$$p_j(t_0, \mu_0) = \frac{\Gamma_j^2 - \left(\frac{\Delta\Gamma_j}{2}\right)^2}{2\Gamma_j} e^{-\Gamma_j t_0} \times \left(\cosh \frac{\Delta\Gamma_j t_0}{2} + \mu_0 \cos \Delta m_j t_0 \right) \quad (1)$$

where $\Delta\Gamma_j = \Gamma_H^j - \Gamma_L^j$, $\Gamma_j = (\Gamma_H^j + \Gamma_L^j)/2$ and $\mu_0 = -1$. For the unmixed case (an initial B_j^0 meson decays as a B_j^0 meson at time t_0), the probability density is given by the above expression with $\mu_0 = +1$. The small effects of CP violation are neglected in the above relation. Unlike $\Delta\Gamma_d$, which can be safely neglected, the width difference in the $B_s^0 - \bar{B}_s^0$ system $\Delta\Gamma_s$ could be as much as 20% of the total width [8].

The above probability is modified by experimental effects. The probability as a function of μ_0 and the reconstructed proper time t is obtained as the convolution of $p_j(t_0, \mu_0)$ with the proper time resolution $\text{Res}_j(t|t_0)$:

$$q_j(t, \mu_0) = N \int_{t_{\min}}^{\infty} p_j(t_0, \mu_0) \text{Res}_j(t|t_0) dt_0$$

with N a normalization factor. Assuming a fraction ω_j of wrong tags at production or decay, the probability becomes:

$$q_j(t, \mu) = (1 - \omega_j)q_j(t, \mu) + \omega_j q_j(t, -\mu) \quad (2)$$

For each signal channel, the background is composed of oscillating B_d^0 mesons with probability given by the expression (2) and of combinatorial background, with probability given by the reconstructed proper time distribution. For a fraction f_j^k of the j component ($j = s, d$, and

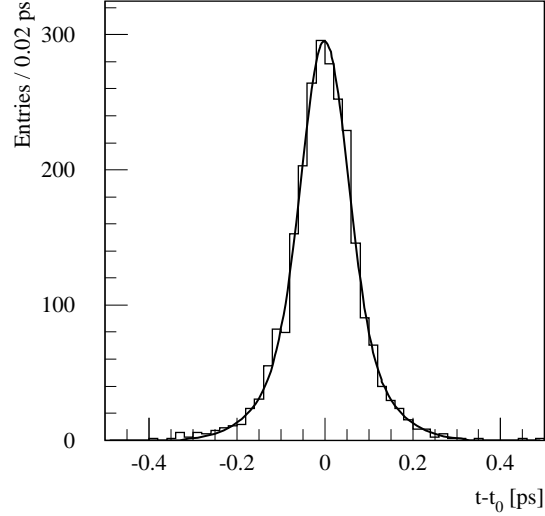


Fig. 5. Proper-time resolution for the decay channel $B_s^0 \rightarrow D_s^- \pi^+$. The curve displays the resolution as obtained from the $\text{Res}(t|t_0)$ function given in the text.

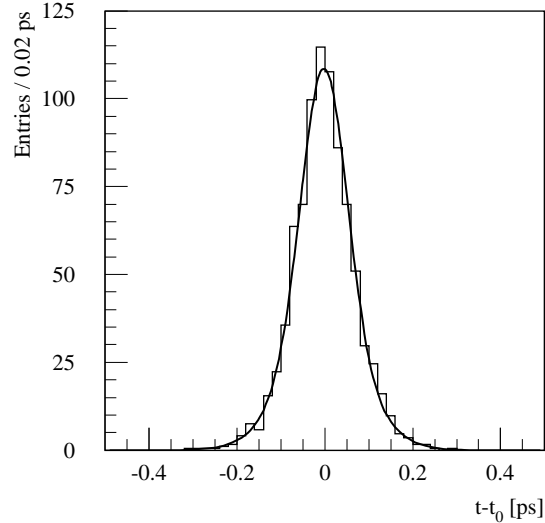


Fig. 6. Proper-time resolution for the decay channel $B_s^0 \rightarrow D_s^- a_1^+$. The curve displays the resolution as obtained from the $\text{Res}(t|t_0)$ function given in the text.

combinatorial background cb) in the total sample of type k , one obtains the probability density:

$$\text{pdf}_k(t, \mu) = \sum_{j=s,d,cb} f_j^k [(1 - \omega_j)q_j(t, \mu) + \omega_j q_j(t, -\mu)]$$

The index $k = 1$ denotes the $B_s^0 \rightarrow D_s^- \pi^+$ channel and $k = 2$ the $B_s^0 \rightarrow D_s^- a_1^+$ channel. The likelihood of the

total sample is written as

$$\mathcal{L}(\Delta m_s, \Delta \Gamma_s) = \prod_{k=1}^{N_{\text{ch}}} \prod_{i=1}^{N_{\text{ev}}^k} \text{pdf}_k(t_i, \mu_i) \quad (3)$$

where N_{ev}^k is the total number of events of type k , and $N_{\text{ch}} = 2$. Each pdf_k was properly normalized to unity.

5 Extraction of Δm_s measurement limits and accuracy

The maximum value of Δm_s measurable in ATLAS was estimated using a simplified Monte Carlo model. The input parameters of this model were: for each signal channel k the number of signal events, N_{sig}^k , the number of background events from B_d^0 decays, $N_{B_d^0}^k$, and the number of events for the combinatorial background, N_{cb}^k ; the characteristics of the events involved in the computation of the proper-time resolution (see below); the wrong-tag fraction. The wrong-tag fraction was assumed to be the same for both B_s^0 and B_d^0 mesons: $\omega_s = \omega_d = 0.22$ (see Ref. [9]). A Monte Carlo sample with $N_{\text{sig}} = N_{\text{sig}}^1 + N_{\text{sig}}^2$ signal events oscillating with a given frequency Δm_s together with $N_{B_d^0} = N_{B_d^0}^1 + N_{B_d^0}^2$ background events oscillating with frequency Δm_d and $N_{\text{cb}} = N_{\text{cb}}^1 + N_{\text{cb}}^2$ combinatorial events (no oscillations), was generated in the following way. For each event with an oscillating b hadron, the true proper time was generated according to an exponential distribution with the slope $[-\Gamma(1 \pm \Delta\Gamma/(2\Gamma))]^{-1}$ which takes into account the contribution of a non-zero $\Delta\Gamma$. Here $\Gamma = \Gamma_s$, $\Delta\Gamma = \Delta\Gamma_s$ for B_s^0 events and $\Gamma = \Gamma_d$, $\Delta\Gamma = 0$ for B_d^0 events. The sign in the slope is chosen according to the contribution of each proper time, corresponding to $\Gamma(1 \pm \Delta\Gamma/(2\Gamma))$, to the exponential decay from Eq. (1), $e^{-\Gamma_j t_0} \cosh(\Delta\Gamma_j t_0/2)$, where the cosh term was factorized from the expression in parentheses and included in the exponential part. The uncertainty on the measurement of the transverse decay length, $\sigma_{d_{xy}}$, and the true value of the g-factor, g_0 , were generated at random according to the distributions obtained from the simulated samples, fitted with appropriate combinations of Gaussian and exponential functions. From the computed true decay length, $d_{xy}^0 = t_0/g_0$, the corresponding reconstructed decay length was generated as $d_{xy} = d_{xy}^0 + S_{d_{xy}} \sigma_{d_{xy}} \Omega$. The reconstructed g-factor was generated as $g = g_0 + g_0 S_g \Omega'$. Both Ω and Ω' are random numbers distributed according to the normal distribution. From the transverse decay length and g-factor, the reconstructed proper time was then computed as $t = g d_{xy}$. The probability for the event to be mixed or unmixed was determined from the t_0 and Δm_s values (Δm_d value if the event was a B_d^0 event) using the expression $(1 - \cos(\Delta m_j t_0) / \cosh(\Delta\Gamma_j t_0/2)) / 2$ left out from Eq. (1) after the exponential part is extracted. For a fraction of the events, selected at random, the state was changed between mixed and unmixed, according to the wrong-tag fraction, ω_{tag} . For the combinatorial background, the reconstructed proper time was

generated assuming that it has the same distribution as the one for B_s^0 mesons. Half of the combinatorial events were added to the mixed events and half to the unmixed events.

5.1 Δm_s measurement limits

The Δm_s measurement limits were obtained applying the amplitude fit method [10] to the ‘data sample’ generated as above. In this method a new parameter, the B_s^0 oscillation amplitude \mathcal{A} , is introduced in the likelihood function by replacing the term ‘ $\mu_0 \cos \Delta m_s t_0$ ’ with ‘ $\mu_0 \mathcal{A} \cos \Delta m_s t_0$ ’ in the B_s^0 probability density function given by Eq. (1). For each value of Δm_s , the new likelihood function is minimized with respect to \mathcal{A} , keeping all other parameters fixed, and a value $\mathcal{A} \pm \sigma_{\mathcal{A}}^{\text{stat}}$ is obtained. One expects, within the estimated uncertainty, $\mathcal{A} = 1$ for Δm_s close to its true value, and $\mathcal{A} = 0$ for Δm_s far from the true value. One defines a 5σ measurement limit as the value of Δm_s for which $1/\sigma_{\mathcal{A}} = 5$, and a sensitivity at 95% confidence limit as the value of Δm_s for which $1/\sigma_{\mathcal{A}} = 1.645$. Limits are computed with the statistical uncertainty $\sigma_{\mathcal{A}}^{\text{stat}}$, and, in some cases, with the total uncertainty $\sigma_{\mathcal{A}}^{\text{total}} = \sigma_{\mathcal{A}}^{\text{stat}} + \sigma_{\mathcal{A}}^{\text{syst}}$. The systematic uncertainty $\sigma_{\mathcal{A}}^{\text{syst}}$ is described in the next section.

5.2 Systematic uncertainties

The systematic uncertainties on the B_s^0 oscillation amplitude $\sigma_{\mathcal{A}}^{\text{syst}}$ are computed as

$$\sigma_{\mathcal{A}}^{\text{syst}} = \Delta\mathcal{A} + (1 - \mathcal{A}) \frac{\Delta\sigma_{\mathcal{A}}^{\text{stat}}}{\sigma_{\mathcal{A}}^{\text{stat}}} \quad (4)$$

where $\Delta\mathcal{A}$ is the difference between the value of the amplitude when a single parameter is changed and the analysis repeated, and the value for the ‘nominal’ set of parameters; $\Delta\sigma_{\mathcal{A}}^{\text{stat}}$ is defined in a similar way.

The following contributions to the systematic uncertainties were considered:

- A relative error of 5% was considered for the wrong-tag fraction for both B_s^0 and B_d^0 .
- The widths of the Gaussian functions from the parametrization of the proper time resolution given in Table 2 were varied by $\pm 1\sigma$.
- The fraction $f_{B_s^0} = BR(\bar{b} \rightarrow B_s^0)$, the B_s^0 lifetime and the Δm_d value were varied separately by the uncertainty quoted in Ref. [11].
- An uncertainty of 5% was assumed for the decay time τ_{cb} of the combinatorial background. The shape remained exponential, only the decay time was modified.

These contributions were added in quadrature to give the systematic uncertainty.

Table 3 shows the dependence of the amplitude and its statistical and systematic uncertainties on Δm_s , as well as the contribution of each component to the systematic

Δm_s	0 ps ⁻¹	5 ps ⁻¹	10 ps ⁻¹	15 ps ⁻¹	20 ps ⁻¹	25 ps ⁻¹	30 ps ⁻¹	35 ps ⁻¹	40 ps ⁻¹
\mathcal{A}	0.0450	-0.1146	0.1892	-0.0337	0.0420	0.0072	-0.2906	0.4318	-0.5406
$\sigma_{\mathcal{A}}^{\text{stat}}$	± 0.0476	± 0.0707	± 0.0895	± 0.1183	± 0.1673	± 0.2456	± 0.3570	± 0.5640	± 0.9300
$\sigma_{\mathcal{A}}^{\text{syst}}$	+0.0967 -0.0838	+0.1285 -0.1018	+0.1297 -0.0960	+0.1468 -0.1144	+0.1796 -0.1424	+0.2035 -0.1580	+0.2980 -0.2264	+0.3674 -0.2658	+0.3636 -0.2592
Systematic contributions									
- wrong-tag fraction	+0.0387 -0.0382	+0.0361 -0.0360	+0.0445 -0.0349	+0.0389 -0.0391	+0.0389 -0.0312	+0.0394 -0.0329	+0.0408 -0.0342	+0.0355 -0.0319	+0.0418 -0.0364
- proper time resolution	+0.0000 -0.0000	+0.0126 -0.0127	+0.0551 -0.0450	+0.0950 -0.0758	+0.1359 -0.1143	+0.1700 -0.1362	+0.2751 -0.2098	+0.3469 -0.2490	+0.3458 -0.2425
- f_s fraction	+0.0884 -0.0742	+0.1227 -0.0943	+0.1086 -0.0773	+0.1049 -0.0761	+0.1107 -0.0790	+0.1035 -0.0724	+0.1069 -0.0780	+0.1146 -0.0861	+0.0888 -0.0661
- B_s^0 lifetime	+0.0038 -0.0036	+0.0009 -0.0009	+0.0034 -0.0032	+0.0030 -0.0033	+0.0060 -0.0000	+0.0146 -0.0076	+0.0010 -0.0014	+0.0132 -0.0088	+0.0372 -0.0390
- Δm_d	+0.0055 -0.0055	+0.0001 -0.0001	+0.0003 -0.0003	+0.0004 -0.0003	+0.0002 -0.0002	+0.0007 -0.0007	+0.0001 -0.0002	+0.0003 -0.0003	+0.0020 -0.0019
- τ_{cb}	+0.0012 -0.0013	+0.0018 -0.0016	+0.0014 -0.0021	+0.0031 -0.0027	+0.0001 -0.0002	+0.0057 -0.0061	+0.0047 -0.0041	+0.0094 -0.0109	+0.0403 -0.0339

Table 3. The oscillation amplitude \mathcal{A} and its statistical and systematic uncertainties as a function of Δm_s for an integrated luminosity of 10 fb⁻¹. The contribution of each component to the systematic uncertainty is also given.

uncertainty for an integrated luminosity of 10 fb⁻¹. In the generated event samples, the value of Δm_s was set to $\Delta m_s^{\text{gen}} = \infty$.

From Table 3, it can be seen that the dominant contributions to the systematic uncertainty come from the uncertainty on $f_{B_s^0}$ fraction and from the parametrization of the proper time resolution.

The uncertainty on $f_{B_s^0}$ fraction has the value given in Ref. [11]. It is, however, expected that the uncertainty will be much smaller at the time this analysis will be done with data. Even now (October 2001), the most up-to-date preliminary value [12] of $f_{B_s^0}$ is 0.099 ± 0.011 , the uncertainty being at the level of 11%, to be compared with the value of 17% used here for the consistency of the data. If one considers the intense activity in B -physics, one can assume that an uncertainty of $\sim 5\%$ will be achieved at the time of data analysis.

The uncertainties on the parameters from the parametrization of the proper time resolution depend on the MC statistics. A larger MC sample can be generated than the one used in this work, in order to reduce these uncertainties. It is therefore reasonable to assume that the uncertainty on the widths from Table 2 can be reduced to half of the actual values.

The systematic uncertainties computed with these ‘projected’ uncertainties are given in Table 4. For the other contributions, the values from Table 3 were used.

The value of the systematic uncertainty as computed here should be considered with caution, as a rough estimate.

5.3 Results

The amplitude as a function of Δm_s for the nominal set of parameters defined in the previous sections, $\Delta\Gamma_s = 0$ and an integrated luminosity of 10 fb⁻¹ is shown in Fig. 7.

Fig. 8 shows the significance of the measurement in units of $\sigma_{\mathcal{A}}$. The 5σ measurement limit is 22.5 ps⁻¹ and the 95% CL sensitivity is 36.0 ps⁻¹, when computed with the statistical uncertainty only. Computed with the total uncertainty, the 5σ measurement limit is 16.0 ps⁻¹ and the 95% CL sensitivity is 34.5 ps⁻¹ for the actual systematic uncertainties, and 21 ps⁻¹ and 35.5 ps⁻¹ for the projected systematic uncertainties.

For an integrated luminosity of 30 fb⁻¹, the 5σ measurement limit is 29.5 ps⁻¹ and the 95% CL sensitivity is 41.0 ps⁻¹, computed with the statistical uncertainty only. The 5σ measurement limit and the 95% CL sensitivity become 18.5 ps⁻¹ and 37.5 ps⁻¹, respectively, for the actual set of systematic uncertainties and 27.0 ps⁻¹ and 40.5 ps⁻¹ for the projected systematic uncertainties.

6 Dependence of Δm_s measurement limits on experimental quantities

Some quantities involved in the measurement of the B_s^0 oscillations are not yet known with enough precision. The cross section for $b\bar{b}$ production could be more than twice the assumed cross section [5]; some decay branching ratios are also not well determined. The value of $\Delta\Gamma_s$ is not yet measured. The characteristics of the detector could be slightly different, depending on the final configuration of the detector. The shape and the fraction of the background will depend, among other factors, on the accelerator luminosity and on the characteristics of the detector. It is therefore necessary to estimate the dependence of the measurement sensitivity for various values of the parameters. The limits presented in this section are computed with the statistical error only.

The dependence of the Δm_s measurement limits on $\Delta\Gamma_s/\Gamma_s$ was determined for an integrated luminosity of 30 fb⁻¹, other parameters having the nominal value. The

Δm_s	0 ps ⁻¹	5 ps ⁻¹	10 ps ⁻¹	15 ps ⁻¹	20 ps ⁻¹	25 ps ⁻¹	30 ps ⁻¹	35 ps ⁻¹	40 ps ⁻¹
\mathcal{A}	0.0450	-0.1146	0.1892	-0.0337	0.0420	0.0072	-0.2906	0.4318	-0.5406
$\sigma_{\mathcal{A}}^{\text{stat}}$	± 0.0476	± 0.0707	± 0.0895	± 0.1183	± 0.1673	± 0.2456	± 0.3570	± 0.5640	± 0.9300
$\sigma_{\mathcal{A}}^{\text{syst}}$	+0.0494 -0.0492	+0.0564 -0.0471	+0.0596 -0.0475	+0.0679 -0.0617	+0.0848 -0.0661	+0.0976 -0.0823	+0.1370 -0.1167	+0.1660 -0.1411	+0.1747 -0.1496
Systematic contributions									
- proper time resolution	+0.0000 -0.0000	+0.0134 -0.0133	+0.0229 -0.0226	+0.0476 -0.0379	+0.0681 -0.0532	+0.0825 -0.0708	+0.1277 -0.1077	+0.1579 -0.1341	+0.1586 -0.1340
- f_s fraction	+0.0299 -0.0301	+0.0412 -0.0272	+0.0321 -0.0226	+0.0285 -0.0287	+0.0316 -0.0238	+0.0305 -0.0242	+0.0278 -0.0286	+0.0333 -0.0265	+0.0252 -0.0205

Table 4. The oscillation amplitude \mathcal{A} and its statistical and systematic uncertainties as a function of Δm_s for an integrated luminosity of 10 fb⁻¹, computed with the ‘projected uncertainties’ on proper time parametrization and on f_s . See the text for details.

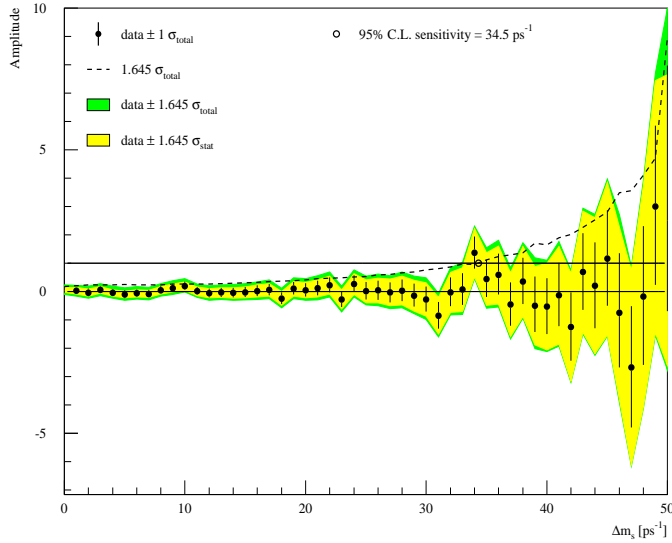


Fig. 7. The B_s^0 oscillation amplitude as a function of Δm_s for an integrated luminosity of 10 fb⁻¹.

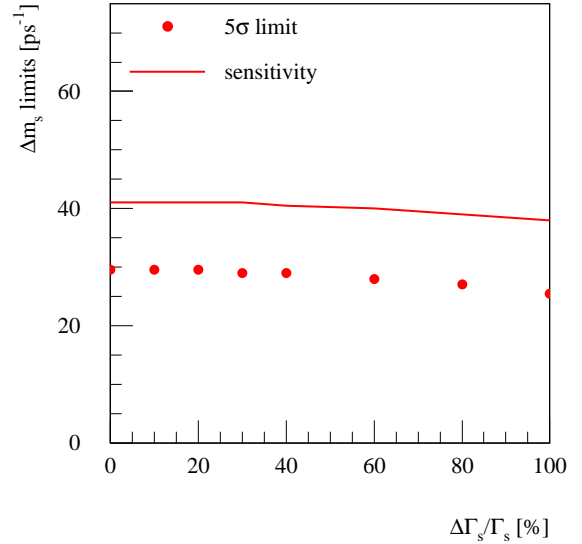


Fig. 9. The dependence of Δm_s measurement limits on $\Delta \Gamma_s / \Gamma_s$.

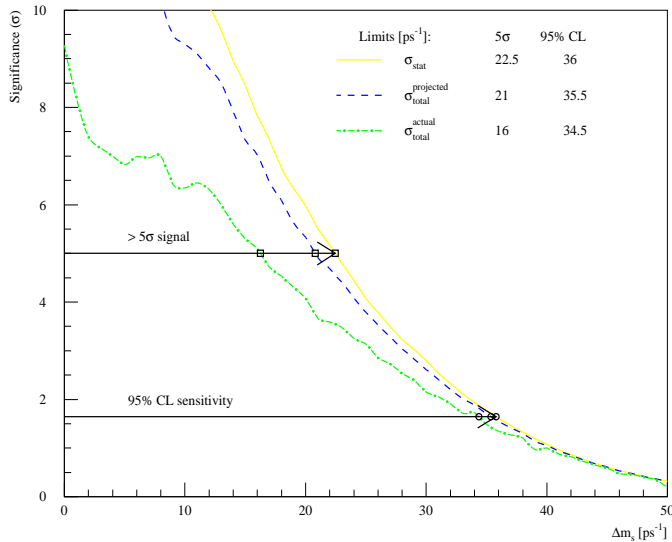


Fig. 8. The measurement significance as a function of Δm_s for an integrated luminosity of 10 fb⁻¹.

$\Delta \Gamma_s / \Gamma_s$ was used as a fixed parameter in the amplitude fit method. The results are shown in Fig. 9 and the numerical values are given in Table 5. No sizeable effect is seen up to $\Delta \Gamma_s / \Gamma_s < 30\%$, therefore $\Delta \Gamma_s$ was set to zero for all other cases.

$\Delta \Gamma_s / \Gamma_s$ (%)	5σ limit (ps ⁻¹)	95% CL sensitivity (ps ⁻¹)
0	29.5	41.0
10	29.5	41.0
20	29.5	41.0
30	29.0	41.0
40	29.0	40.5
80	27.0	39.0
100	25.5	38.0

Table 5. The dependence of Δm_s measurement limits on $\Delta \Gamma_s / \Gamma_s$.

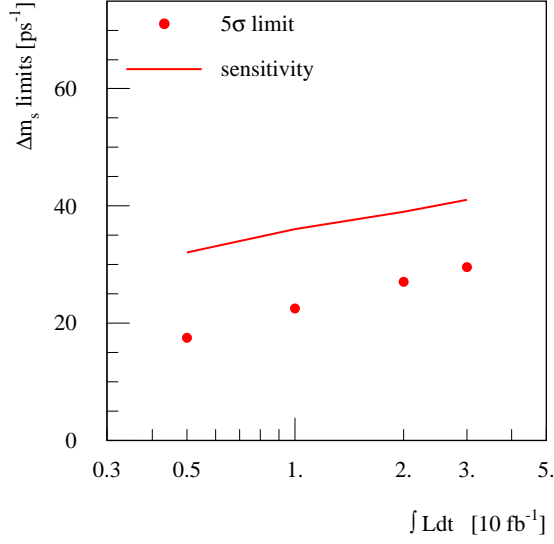


Fig. 10. The dependence of Δm_s measurement limits on the integrated luminosity.

The dependence of the Δm_s measurement limits on the integrated luminosity is shown in Fig. 10, with the numerical values given in Table 6.

Luminosity (fb^{-1})	5 σ limit (ps^{-1})	95% CL sensitivity (ps^{-1})
5	17.5	32.0
10	22.5	36.0
20	27.0	39.0
30	29.5	41.0

Table 6. The dependence of Δm_s measurement limits on the integrated luminosity.

The shape and the fraction of the combinatorial background were varied within reasonable values. It was assumed that the shape remains exponential and only the decay time was modified. The number of events for the combinatorial background was varied within $\pm 50\%$ of the number determined in Section 2, keeping the number of B_s^0 and B_d^0 events to the nominal values. The dependence of the Δm_s measurement limits on the decay time of the combinatorial background is shown in Fig. 11, with the numerical values given in Table 7, while the dependence on the number of events is given in Fig. 12 and Table 8.

7 Accuracy of the Δm_s measurement

For Δm_s values smaller than the 5 σ measurement limit, the expected accuracy is estimated using the log-likelihood method, with the likelihood function given by Eq. (3). In the fit, the Δm_s value was free, while the other parameters were fixed to their nominal values. An example of the

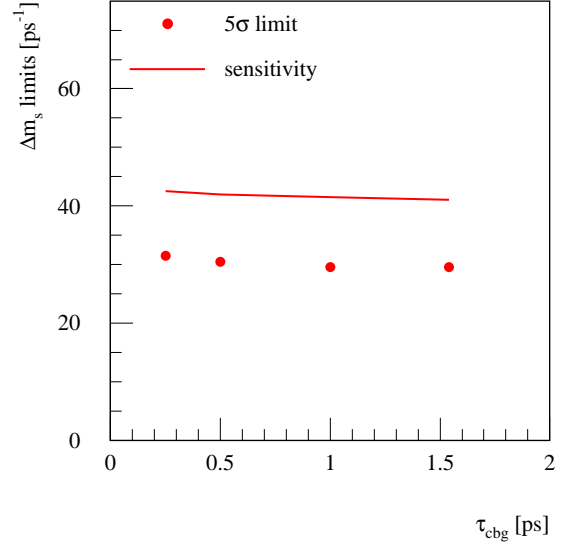


Fig. 11. The dependence of Δm_s measurement limits on the decay time of the combinatorial background, assuming an exponential decay.

τ_{cbg} (ps)	5 σ limit (ps^{-1})	95% CL sensitivity (ps^{-1})
0.25	31.5	42.5
0.50	30.5	42.0
1.00	29.5	41.5
1.54	29.5	41.0

Table 7. The dependence of Δm_s measurement limits on the decay time of the combinatorial background, assuming an exponential decay.

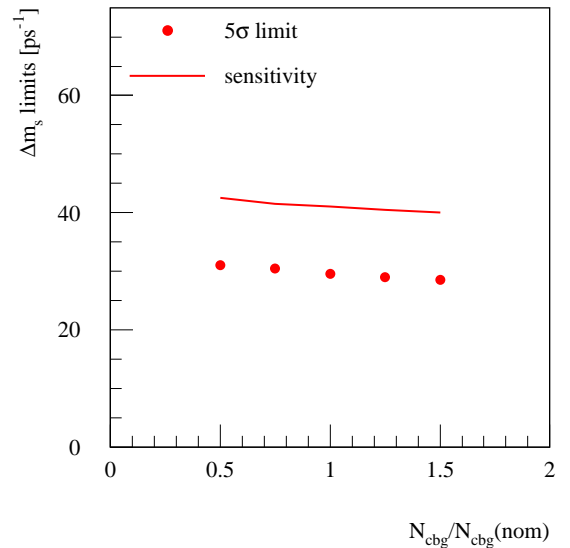


Fig. 12. The dependence of Δm_s measurement limits on the number of events for the combinatorial background.

$N_{\text{cbg}}/N_{\text{cbg}}^{\text{nom}}$	5σ limit (ps ⁻¹)	95% CL sensitivity (ps ⁻¹)
0.50	31.0	42.5
0.75	30.5	41.5
1.00	29.5	41.0
1.25	29.0	40.5
1.50	28.5	40.0

Table 8. The dependence of Δm_s measurement limits on the number of events for the combinatorial background.

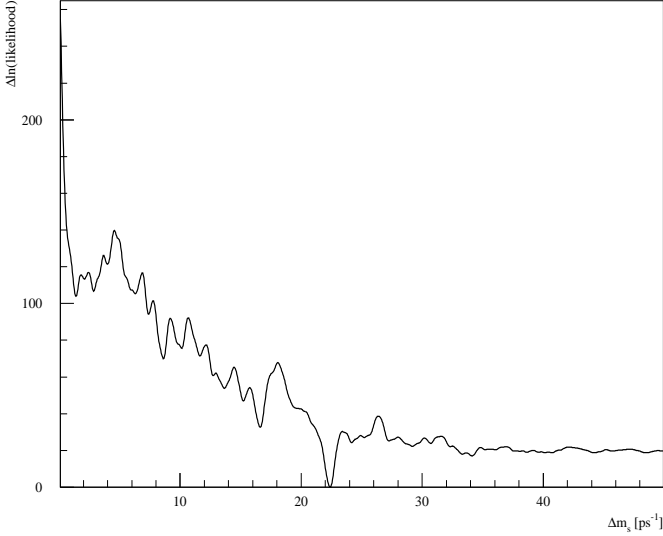


Fig. 13. The negative log-likelihood function for an integrated luminosity of 10 fb⁻¹ and a generated $\Delta m_s^{\text{gen}} = 22.5$ ps⁻¹.

likelihood function is given in Figure 13 for an integrated luminosity of 10 fb⁻¹ and a generated $\Delta m_s^{\text{gen}} = 22.5$ ps⁻¹.

The accuracy was determined for different values of the integrated luminosity. The results are given in Table 9.

The systematic accuracy of the Δm_s measurement was obtained similarly to the systematic uncertainty on the measurement limits: one parameter was changed, keeping the other fixed to their nominal values, and the analysis was repeated. The difference between the value of the fitted Δm_s parameter when a single parameter is changed and the analysis repeated, and the value for the ‘nominal’ set of parameters was taken as the systematic contribution corresponding to that parameter. The total systematic uncertainty is the quadratic sum of the individual contributions. The parameters changed are the same as for the measurement limits, see Section 5.2, within the ‘actual’ uncertainties.

One can see from Table 9 that the Δm_s measurement, if within the reach of the ATLAS detector, will be dominated by the statistical errors.

8 Conclusions

In this note, the performance of the ATLAS detector to measure the B_s^0 oscillations was estimated using Monte

Luminosity (fb ⁻¹)	Δm_s^{gen} (ps ⁻¹)	$\Delta m_s^{\text{rec}} \pm \sigma_{\text{stat}}^{\Delta m_s} \pm \sigma_{\text{syst}}^{\Delta m_s}$ (ps ⁻¹)	Obs.
5	17.5	$17.689 \pm 0.083 \pm 0.002$	5σ limit
10	15.0	$15.021 \pm 0.049 \pm 0.002$	5σ limit
	22.5	$22.396 \pm 0.072 \pm 0.005$	
20	15.0	$14.949 \pm 0.033 \pm 0.002$	5σ limit
	20.0	$20.041 \pm 0.068 \pm 0.005$	
	27.0	$26.948 \pm 0.070 \pm 0.003$	
30	15.0	$14.942 \pm 0.028 \pm 0.004$	5σ limit
	20.0	$20.010 \pm 0.043 \pm 0.002$	
	29.5	$29.708 \pm 0.083 \pm 0.007$	

Table 9. The accuracy of Δm_s measurement as a function of the integrated luminosity. $\sigma_{\text{stat}}^{\Delta m_s}$ represents the statistical uncertainty, $\sigma_{\text{syst}}^{\Delta m_s}$ the systematic uncertainty.

Carlo simulated events, propagated through a detailed simulation of the detector. For an integrated luminosity of 10 fb⁻¹, a 5σ measurement will be possible up to 22.5 ps⁻¹, the experiment being 95% CL sensitive up to 36.0 ps⁻¹. These limits increase to 29.5 ps⁻¹ and 41.0 ps⁻¹, respectively, for an integrated luminosity of 30 fb⁻¹. The effect of the systematic uncertainties on the measurement limits is rather limited, if the precision of the $f_{B_s^0}$ fraction is improved with respect to the actual value, and if enough Monte Carlo events are generated for the parametrization of the proper time.

If the Δm_s value will be within the ATLAS reach, the measurement will be dominated by the statistical error. A total uncertainty of the order of ~ 0.07 ps⁻¹ is expected for a value of $\Delta m_s = 22.5$ ps⁻¹ for an integrated luminosity of 10 fb⁻¹, the total uncertainty decreasing to ~ 0.04 ps⁻¹ for a luminosity of 30 fb⁻¹.

The dependence of the measurement sensitivity on various parameters which will be known only at the time of the data analysis was also evaluated.

The values obtained in this note for the measurement limits and accuracies should be re-evaluated at a later time, taking into account the changes in the detector geometry and in the simulation and reconstruction software.

Acknowledgements. This work has been performed within the ATLAS collaboration, and we thank collaboration members for helpful discussions. We have made use of the physics analysis framework and tools which are the result of collaboration-wide effort. The authors would like to thank P. Eerola and N. Ellis for fruitful discussions, and E. Kneringer for computing support. The work was supported by the Federal Ministry of Education, Science and Culture, Austria.

References

1. F. Parodi, P. Roudeau and A. Stocchi, *Nuovo. Cim.* **A112** (1999) 833.
2. The LEP B Oscillation Working Group, *Combined Results on B_s^0 oscillations: Results for BEAUTY 2000 Conference* (2000).

3. Particle Data Group: D.E. Groom et al., *Review of Particle Physics*, Euro. Phys. J. C**15** (2000) 1.
4. T. Sjöstrand, Comp. Phys. Comm. **82** (1994) 74.
5. The ATLAS Coll., *ATLAS Detector and Physics Performance Technical Design Report*, CERN/LHCC/99-14 (1999).
6. *Upper Tail Probability of Chi-Squared Distribution*, CERNLIB - CERN Program Library, routine entry PROB (G100), CERN.
7. J. Baines et al., *B-Physics Event Selection for the ATLAS High Level Trigger*, ATL-DAQ-2000-031 (2000).
8. M. Beneke, G. Buchalla and I. Dunietz, Phys. Rev. D**54** (1996) 4419; M. Beneke et al., Phys. Lett. B**459** (1999) 631.
9. P. Eerola et al., *Asymmetries in B decays and their experimental control*, ATL-PHYS-94-054 (1994).
10. H.G. Moser and A. Roussarie, Nucl. Instr. Meth. A**384** (1997) 491.
11. Particle Data Group: C. Caso et al., *Review of Particle Physics*, Euro. Phys. J. C**3** (1998) 1.
12. The LEP Working group on B oscillations, *Combined results for Budapest, EPS-HEP 2001*.
<http://lepibosc.web.cern.ch/LEPBOSC/>